OPTOELECTRONICS AND ADVANCED MATERIALS – RAPID COMMUNICATIONS Vol. 7, No. 11-12, November - December 2013, p. 1002-1010

New generation WIMAX antenna based on metamaterial superstrate

E. DOĞAN, E. UNAL*, D. KAPUSUZ
Electric-Electronic Engineering Department, University of Mustafa Kemal, İskenderun, Hatay, Turkiye

In this study, a microstrip patch antenna system based on metamaterial superstrate (PAMS) is proposed. Patch antennas suffer from low gain and directivity. A significant study is realized to circumvent this drawback by implementing a patch antenna based on metamaterial superstrate. The effective medium parameters of the unit cell are retrieved and planar three-layer metamaterial composed of unit cell arrays are used as a superstrate for gain and directivity enhancement of a microstrip patch antenna at 5.6 GHz. The gain and directivity efficiency of the proposed system is about 13.474 dB and 12.40 dB, respectively at 5.6 GHz. In this study, Simulation and measurement results are also presented. The PAMS consists of periodically arranged metamaterial array unit cells as a superstrate and patch antenna. The system is designed to operate from 5.2 GHz to 6 GHz with a return loss of -32.174 dB at first mode (5.6 GHz). Both simulation and measurement results of the PAMS show that this configuration is able to realize a broadside gain 72% of the maximum gain from the metamaterial superstrate. The effects of the compactness of the arrays are also investigated. It is observed that return loss is directly proportional with the compactness of the superstrate. The maximum return loss (-32.174 dB) is obtained with seven arrays of metamaterial.

(Received July 1, 2013; accepted November 7, 2013)

Keywords: Metamaterials, Antenna, Split Ring Resonator, Kramers-Kronig

1. Introduction

Artificial materials that exhibit unusual physical properties attracted much attention in the last decade of the last century [1]. Improvement of some prescribed antenna features such as impedance matching, gain, bandwidth, efficiency, front-to-back ratio can be realized by using artificial materials and surfaces. These features may represent a novel way to overcome the limitations shown by some of the known techniques for reducing the antenna size [2]. Many researchers are studying to improve the gain of microstrip antennas since this type of antenna is desired for its low cost properties but with the compromise in the gain and directivity [3].

Many papers have been published regarding the LH MTMs integrated with antennas, and their properties have been analyzed and investigated. Song et al [4] investigated a patch antenna based on I-shaped left-handed materials by using the method of finite difference time domain (FDTD). They provided higher antenna gain, a lower return loss, and a better improvement of the antenna's characteristics due to LH MTMs. Fladie and Bernhard [5] theoretically examined the source fields and radiation characteristics of left and right handed microstrip patch antenna designs. They further investigated these properties by using equivalence theory and an approximate radiating slot model. Their study indicates that the use of LH MTMs results in an electrically small antenna with an omni-directional rather than a broadside radiation pattern when operated in the first resonant mode. Majid et al [6] simulated and fabricated a new type of LH MTM microstrip antenna. The structure is combined of the modified square rectangular split ring resonators and capacitively loaded strips. They indicated that the performance of the antenna can be improved where the gain of the microstrip antenna is increased up to 4 dB, and its bandwidth widens from 2.9% to 4.98%. Han et al [7] discussed design, simulation, fabrication and measurement of LH MTM microstrip antennas. Their structure is combined of square rectangular split ring and thin wire. They showed that the return loss is improved by 9.62 dB and 12.29 dB in the simulation and measurement results, respectively.

In this work, a study has been made to discuss and analyze the properties of the LH MTM microstrip patch antenna structure. Besides, performance of microstrip antenna with and without LH MTM are compared and evaluated. Designed and fabricated antenna has a unique feature that the return loss, voltage signal wave ratio and electric field radiation pattern of the patch antenna are enhanced by using metamaterial superstrate. Also, the experimental results are in good agreement with that of the numerical simulations.

2. Characterization of metamaterial unit cell using effective medium theory

In the first step of the study, a metamaterial unit cell (Fig.1.a) is designed as the building block of the antenna superstrate. The unit cell is composed of rectangular split ring resonator (SRR) and metallic strip wire (SW) to realize negative permeability and permittivity, respectively. While SRRs are printed on one side of the FR4 epoxy substrate with a thickness of 1.6mm, relative

dielectric permittivity ε_r=4.4, relative magnetic permeability μ_r=1 and loss tangent δ_ε=0.02, SW inclusions are printed on the other side of the substrate. A set of design parameters illustrated in Fig. 1a and Table 1 describes the dimensions of the SRR and SW inclusions. These parameters of the inclusions provide us to design a metamaterial with simultaneous negative permittivity and permeability at the operating frequency region of the antenna. The effective medium parameters of the periodic structure are extracted by using the Nicolson Ross Weir technique (NRW) [8,9] from the scattering parameters which are evaluated with two different commercial EM solvers (HFSS and CST). HFSS and CST are operated together to compare the results with each other. The NRW technique is converted into macros in both Simulation techniques hence optimization procedure for the dimensions of the SRR and SW can smoothly be performed in both CST and HFSS frameworks.

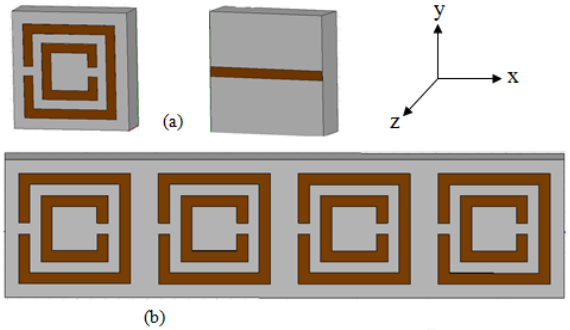

Fig. 1. The geometry of the unit cell (a) The simulation setup for the transmission and reflection analysis of the metamaterial unit cell (b).

The constitutive effective permeability (μ_r) and permittivity (ε_r), effective refractive index (***n***) for the SRR-SW metamaterial unit cell are extracted from the NRW relations in the case of normal incidence.

$$\mu_r = \frac{1+\Gamma_1}{\wedge(1-\Gamma)\sqrt{\frac{1}{\lambda_0^2}-\frac{1}{\lambda_C^2}}}, \quad \frac{1}{\wedge^2} = -\left[\frac{1}{2\pi L}\ln\left(\frac{1}{T}\right)\right]^2 \tag{1}$$

$$\varepsilon_r = \frac{\lambda_0^2}{\mu_r}\left(\frac{1}{\lambda_C^2} - \left[\frac{1}{2\pi L}\ln(\frac{1}{T})\right]^2\right), \quad T = \frac{S_{11}+S_{21}-\Gamma_1}{1-(S_{11}+S_{21})\Gamma_1}$$

$$Z = \sqrt{\frac{(1+S_{11})^2 - S_{21}^2}{(1-S_{11})^2 - S_{21}^2}}$$

$$n = \frac{j}{k_o d}\ln\left(\frac{S_{21}}{1-S_{11}\frac{Z-1}{1+Z}}\right)$$

where λ_0 and λ_c refer to the wavelength in free space and cutoff wavelength, respectively. Wave impedance (***Z***) and the refractive index (***n***) are calculated in terms of scattering parameters S_{11} and S_{21}which represent reflection and transmission coefficients, respectively. Using the values of ***Z*** and ***n*** obtained in Eq.1. The effective dielectric permittivity and magnetic permeability can be calculated using the equations; ε_{eff} = ***n***/***Z*** and μ_{eff} = ***nZ***.

Real part of the complex refractive index has multiple solutions. Only one of the solutions has physical meaning due to the uniqueness theorem which is supported by the Kramers-Kronig relations. The real part of the complex effective refractive index can be obtained using

$$n_{eff}(\varpi) = 1 + \frac{2}{\pi} P \int_0^\infty \frac{\omega k_{eff}(\omega)}{\omega^2 - \varpi^2} d\omega \tag{2}$$

where ***P*** defines the principal value of the integral. Upper limit of the integral is selected as infinite due to the uncertainty of the imaginary part of the refractive index throughout the entire domain.

Modeling of the metamaterial unit cell in simulation is shown in Fig. 1.b. Since the structure is periodic along x and z directions, it is adequate to assign the boundary conditions as perfect electric conductor in the x direction and perfect magnetic conductor in the z direction to evaluate the scattering parameters below the diffraction frequencies. PEC and PMC are characterized by vanishing tangential electric field and magnetic fields at these surfaces, respectively. Each simulation model consists of a two-port waveguide formed by a pair of both PEC and PMC walls. PEC type boundary conditions are applied at those surfaces of the computational volume which are perpendicular to the incident electric field vector. Similarly, PMC type boundary conditions are applied at those surfaces of the computational volume which are perpendicular to the incident magnetic field vector. The boundary conditions along y direction are assigned as perfectly matched absorbers. The SRR-SW unit cell is positioned in the rectangular air filled waveguide which is excited by the transverse electromagnetic (TEM) mode with propagation vector **k** parallel to the SRR-SW surface, electric field E is along the SW surface and magnetic field H is perpendicular to the SRR surface.

The scattering parameters are evaluated over the frequency range of 1-10 GHz, hence all of the effective parameters for the metamaterial can be observed around 5.6 GHz frequency region by using the extraction procedure. The optimization is operated to get negative medium parameters at 5.6 GHz for WIMAX applications. Whereas the phase of the waveport in the y direction is embedded to the surface of the metamaterial, that of the waveport in the y direction is assigned to 1mm above the metamaterial to provide a proper separation between the antenna and metamaterial which will be used as superstrate in the antenna system. To evaluate the optimized values of the metamaterial (Table 1), we defined the SRR-SW dimensions as parametric variables and optimized the unit cell by Interpolated Quasi Newton Approach in HFSS. The optimized dimensions of SRR and SW for negative effective permittivity and permeability around 5.6 GHz are tabulated in Table 1 where $\boldsymbol{a_x}$ and $\boldsymbol{a_y}$ are unit cell dimensions. In Table 1, ***d*** represents the thickness of the unit cell, ***a*** and ***r*** are the width of metallic strips on the front and back sides respectively.

Table 1. Optimized dimensions of the metamaterial unit cell superstrate.

a_x(mm)	a_y(mm)	d(mm)	a(mm)	r(mm)
5	5	1.6	0.4	0.017

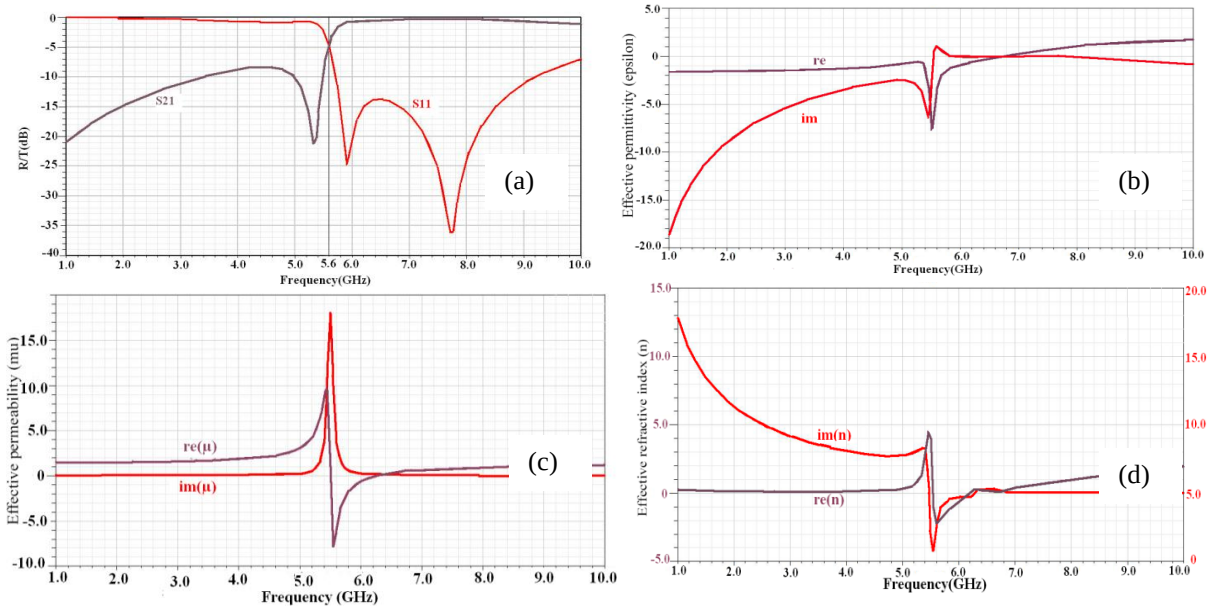

Fig. 2. Results of the optimized SRR-SW LHM unit cell a)transmission (S_{21}) and reflection (S_{11}) parameters b) the real and imaginary parts of the effective dielectric constant, c) the real and imaginary parts of effective magnetic permeability, d) the real and imaginary parts of negative refractive index.

Fig. 2.a indicates Ansys HFSS simulation results of the scattering parameters S_{11} and S_{21}. The scattering parameters start to change in the vicinity of 5.6 GHz. The evaluated real and imaginary values of effective electric permittivity, effective magnetic permeability and refractive index extracted from simulated scattering parameters are shown in Fig. 2.b, Fig.2.c and Fig.2.d, respectively. It is obviously shown that around 5.6 GHz each effective parameter of the periodic structure is below zero. It means, negative medium parameters are realized at this frequency. Therefore, the metamaterial that exhibits negative refractive index at the operating frequency of WIMAX application will be designed and operated with metallic patch antenna.

3. Design of antenna and SRR-SW based metamaterial

The Microstrip patch antenna is chosen in this work due to the performance, robust design, fabrication and extent usage. It has several applications, such as, Mobile and satellite communication, Global Positioning Systems, Radio Frequency Identification (RFID), Worldwide Interoperability for Microwave Access (WiMax), Radar, Rectenna, Telemedicine and Medical applications [10].

Microstrip line feed is chosen as supplier because it is one of the easier methods to fabricate. It is just a conducting strip connecting to the patch and source; hence it can be considered as extension of patch. The coaxial cable to microstrip transition is realized by soldering the 50Ω SMA connector. The inner conductor of the coaxial cable is attached to the radiation patch of the antenna by microstrip line feed while the outer conductor is connected to the copper ground plane. Advantages of coaxial feeding are easy fabrication, impedance matching and low spurious radiation. Beside this, narrow bandwidth is the main disadvantage. The complete geometry of the proposed patch antenna is shown in Fig. 3 where a copper plate on FR4-epoxy substrate with dimensions of Lg x Wg is used as a ground plane.

	Size	Unit
Operating frequency	5.6	GHz
Patch length(L)	25	mm
Patch width (W)	24	mm
Plate length (Lg)	50	mm
Plate width (Wg)	50	mm
Feed	Microstrip line feed	-
Feed line width	2	mm
Feed line length	21	mm
Plate thickness	1.6	mm

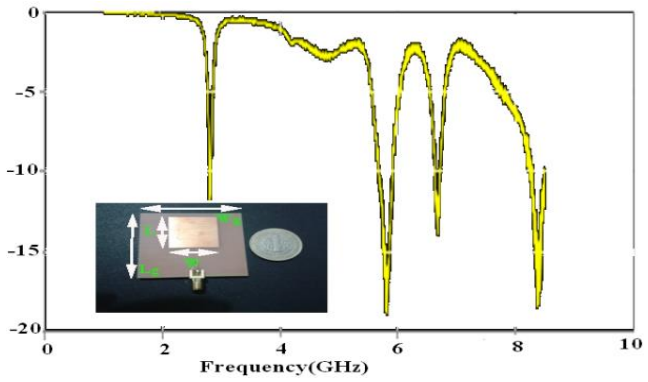

Fig. 3. Measured return loss of manufactured patch antenna (inset) fed by microstrip line with 5.6 GHz operating frequency and its dimensions.

The proposed antenna geometry is analyzed by using Ansys HFSS and CST. It is clearly observed that the return loss results have similar characteristics. As shown in Fig. 4, the return loss S_{11} of the patch antenna is -28.1587 dB and -25.15 dB at 5.6 GHz for Ansoft HFSS and CST microwave studio, respectively. The microstrip patch antenna also demonstrates good return loss at 6.3 GHz. The return loss is smaller (S11 ≤ -10dB) than the threshold level and the peak gain is obtained around - 17.5 dB for 6.3 GHz. The return loss of the manufactured microstrip line feed patch antenna is measured using ENA Series Network Analyzer (E5071B). The measured return loss S_{11} at 5.6 GHz is approximately -18.7 dB. The experimental results are in good agreement with the simulation results. The return loss at 6.3 GHz is also smaller ($S_{11} \leq$ -10 dB) than the threshold level in measurement. Beside this, one another good return loss below -10 dB is observed at 2.8 GHz. It can be concluded that the patch antenna has three different radiation frequency bands. The measurement of the reflection is achieved by surrounding the antenna with absorbers. Calibration of the system is achieved using a void hole, an absorber, and a PEC reflector situated in this absorber. The calibrated reflection coefficient is evaluated by;

$$S_{11}^{cal} = \frac{S_{11} - S_{11}^{abs}}{S_{11}^{pec} - S_{11}^{abs}}, \quad \arg(S_{11}^{cal}) = \arg(S_{11}) - \arg(S_{11}^{pec}) - \pi \qquad (3)$$

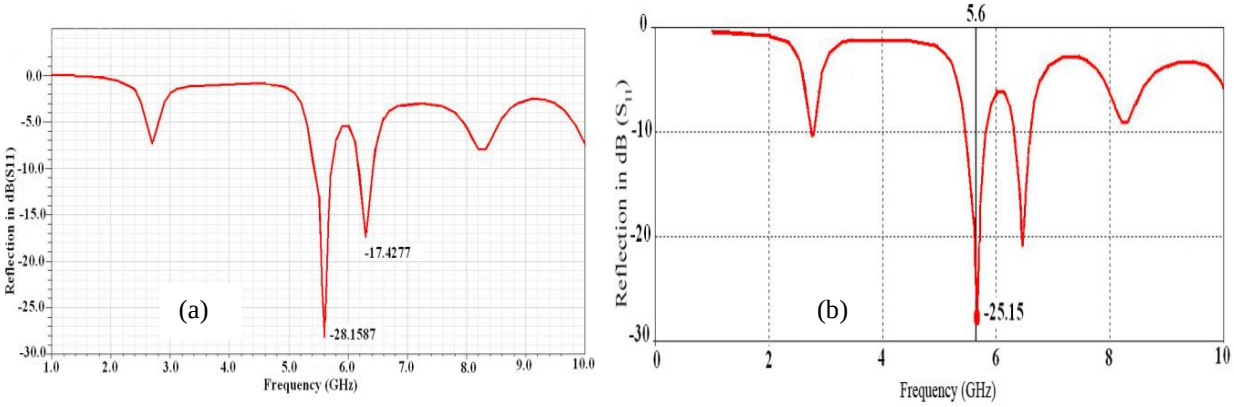

Fig. 4. Return loss of simulated original microstrip line feed patch antenna by HFSS (a) and CST(b).

The SRR-SW metamaterial structure presented in the second section is involved as a superstrate for the microstrip patch antenna operating at 5.6 GHz to improve the return loss and antenna gain. The side views of the constructed metamaterial which will be used in the patch antenna metamaterial system (PAMS) are shown in Fig. 5.a. The superstrate consists of one layer which includes seven unit cells as shown in Fig. 5.b. Each unit cell contains four SRR elements supported by a FR4-epoxy substrate having metallic strip wire (SW) on the back side. The width of metallic strip wire is 0.017 mm. Different numbers of DNG elements are also attempted, but unit cell with four DNG elements gives the best gain. The superstrate is mounted above the antenna using four plastic bolts at the corners. The spacing between the radiation source and the bottom of the superstrate is 1.5 mm. While

SRR cells are excited by magnetic field which directs along the center of metal rings, SW cells are excited by electric field polarized along SW. The poynting vector of the radiated signal is perpendicular to the surface of the patch antenna. The PAMS is positioned in such a way that the strip wire of the metamaterial unit cell and the electric field created by the patch are oriented in the same direction. All the microstrip patches in the simulations and measurements are fed by a microstrip line with 1.6 mm width, corresponding to an input impedance of 50Ω.

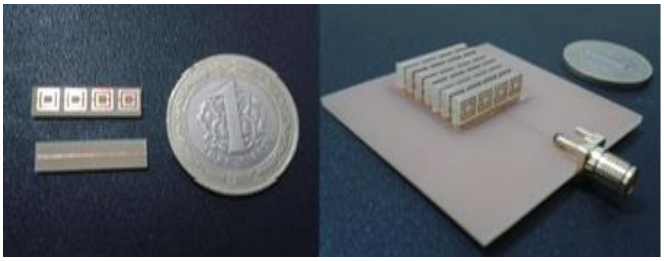

(a) (b)

Fig. 5. Front and back view of one array of metamaterial (a) and fabricated PAMS with seven arrays (b).

PAMS shown in Fig. 5 is designed using Ansys HFSS and CST microwave studio. The simulation results are also compared with those of the measurement obtained by ENA Series Network Analyzer (E5071B model). There are some differences between the measured and the simulated results that come from measurement errors and manufacturing processes. The return loss of the PAMS at 5.6 GHz frequency decreases down to -35.1113 dB (in HFSS) and -32.21 dB (in CST) (Fig. 6). While the return loss of the patch antenna without metamaterial is -28.1587 dB and -25.12 dB for Ansys HFSS and CST microwave studio, respectively, the return loss of the PAMS simulated at 5.6 GHz frequency has significantly reduced by an amount of -6.9526 dB (HFSS) and -7.09 dB (CST), respectively. Beside this, the measured return loss is about -13.474 dB less than the free space patch antenna.

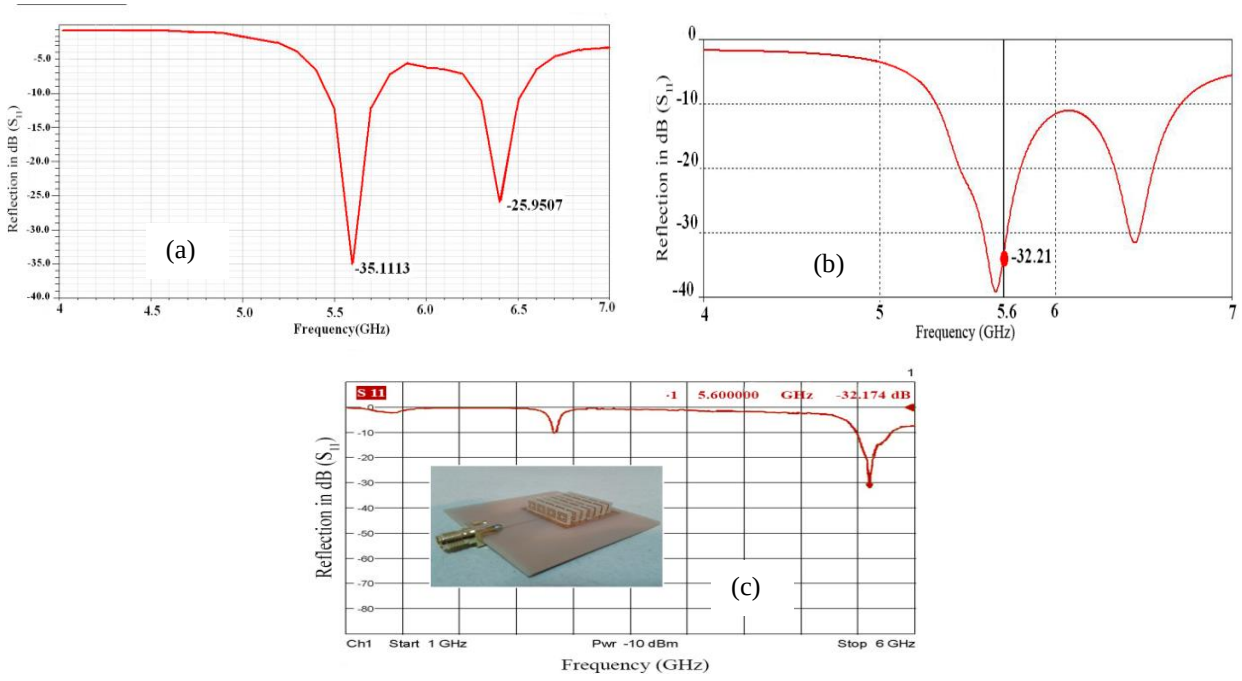

Fig. 6. The return loss of PAMS simulated in HFSS(a), in CST (b) and measured (c).

It can be concluded that %41.18 improvement is possible on the value of the return loss of the patch antenna with PAMS. The return loss enhancement results of the patch antenna with and without metamaterial is given in Table 2. Beside this, the return loss enhancement is also provided for the other radiation frequencies observed in both simulation and measurement results. While the return loss of the patch antenna without metamaterial at 3 GHz is about -10 dB, that of the PAMS is below -15 dB. It means the PAMS is not only used for the enhancement of return loss but also it can be used to reduce the electrical dimensions of the antennas. The metamaterial also provides wider bandwidth. While the bandwidth of the patch antenna without metamaterial is only 0.35 GHz, PAMS has much wider bandwidth of 0.8 GHz around 5.6 GHz frequency.

Table 2. Comparison of simulation and measurement results of the PAMS return loss at 5.6 GHz.

	Ansys HFSS results(S11)	*CST results (S11)*	*Measurement results*
Patch antenna fed by a strip line	-28.16 dB	-25 dB	-18.70 dB
Gain decreases	-35.11 dB	-32.2 dB	-32.17dB
PAMS	-6.95 dB	-7.09 dB	-13.47 dB

4. PAMS with nonperiodically Arranged MTM

The effects of the non-periodically arranged metamaterials on return loss of microstrip patch antenna are also investigated. In the first design, only two arrays of PAMS are used as shown in Fig. 7.a and 7.b. In the second arrangement shown in Fig. 7.c and 7.d, one of the periodic structure is shifted to the other edge of the patch antenna.

The effects of two metamaterial arrays as superstrate on antenna return loss is shown in Fig. 7. The metamaterial is mounted on the patch antenna with different arrangements. The distance between two metamaterial array is 3.4 mm for first arrangement and 20 mm for second arrangement. The dimensions of the SRR-SW inclusions are selected to achieve negative effective refractive index at 5.6 GHz (Table 1). While the return loss value is -17.497 dB for the first arrangement, that of the second arrangement is -21.4 as in Fig.7.b and 7.c. Beside this, superstrate with two metamaterial arrays shown in Fig.7.a and 7.b have better return loss compared to superstrate with one metamaterial array. The enhancement of the return loss results from the better behavior of the arrangement as metamaterial. When the metamaterial arrays are close to each other, the overall structure behaves as a homogeneous material at least for some particular frequency bands of the EM waves radiated from patch antenna. The measurement results are in good agreement with that of simulations.

The effects of four and seven metamaterial arrays on antenna return loss are obtained and shown in Fig. 8. The PAMS are placed on the patch antenna with different arrangements. The distance between two metamaterial arrays is 6 mm for the first arrangement and 3.4 mm for the second arrangement. The dimensions of the SRR-SW inclusions are also selected to realize negative effective medium characteristics at 5.6 GHz. While the return loss of the PAMS is -29.565 dB for the first arrangement with four metamaterial arrays, that of the second arrangement with seven metamaterial arrays is -32.174 dB. In addition, the return loss of four and seven metamaterial arrays is about -6 dB lower than that of two metamaterial array. Beside this, the resonance shown at 2.8 GHz frequency is also improved by seven array PAMS which can be used as two band antennas. This means that the PAMS can also be used to achieve electrically small antenna. The enhancement of the return loss for seven arrays of PAMS with respect to four arrays of PAMS results from the better attitude of the system as an effective material. It means, while the distance between the arrays of metamaterial decreases, the PAMS behaves as a homogeneous material for some frequency bands of the EM waves radiated from the patch antenna.

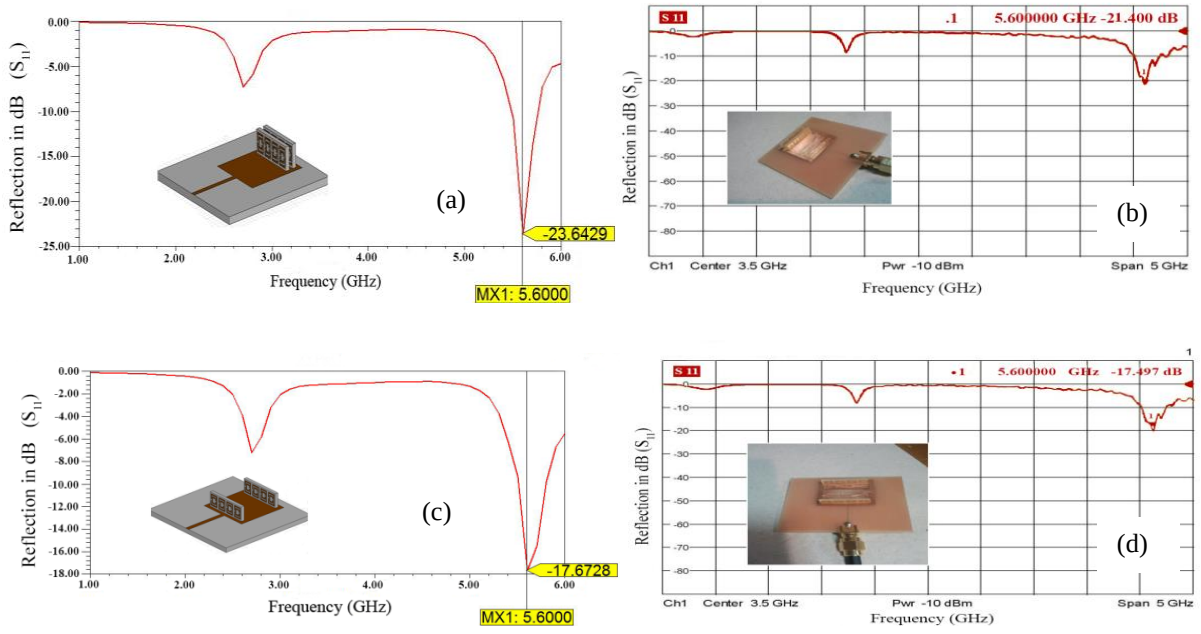

Fig. 7. Return loss of two arrays of front row in HFSS(a) in measurement (b)and return loss of metamaterial arrays at two edges in HFSS (c) and in measurement (d).

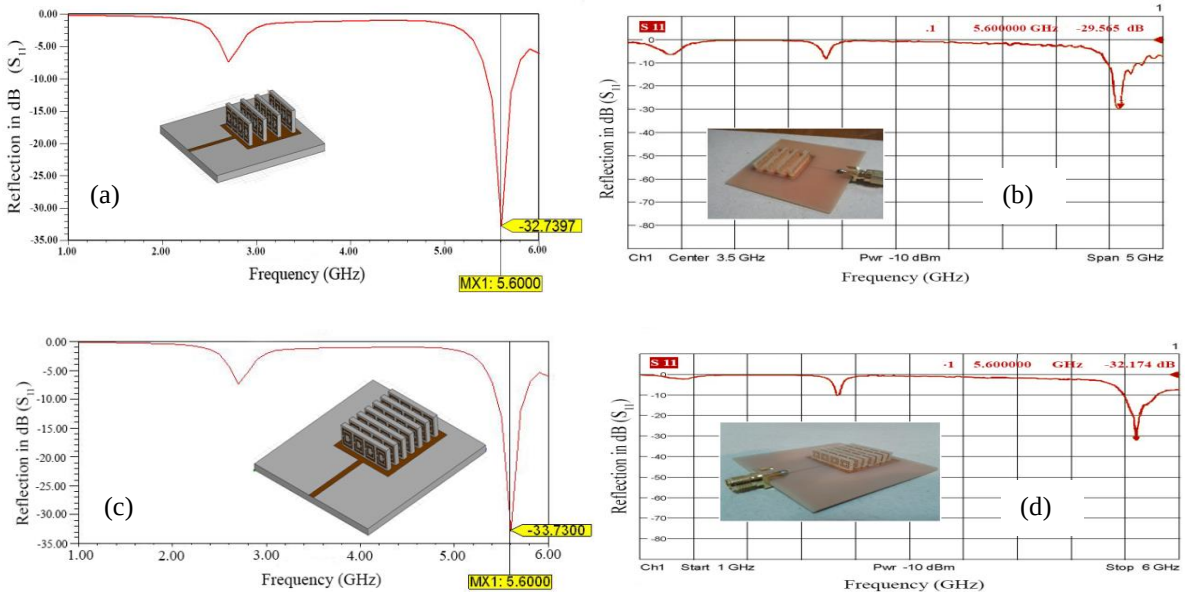

Fig. 8. Return loss of four arrays of metamaterials in HFSS(a) in measurement (b)and return loss of seven arrays of metamaterials in HFSS (c) and in measurement (d).

As a last comparison, the effects of the width of three metamaterial arrays on the return loss are investigated as shown in Fig. 9. In Fig. 9.a and 9.b the PAMS are distributed uniformly over the entire surface of the patch antenna. The PAMS in Fig. 9.c and 9.d are also distributed uniformly over the surface of the patch antenna but the widths of the metamaterial arrays exceed the border of the patch antenna. The distance between two metamaterial arrays is 8 mm for each arrangement. While the return loss of the PAMS is -20.462 dB for the first arrangement, that of the second arrangement is -22.305 dB at 5.6 GHz. The return loss of the second arrangement shown in Fig. 9.c and 9.d is better than that of the first arrangement shown in Fig 9.a and 9.b due to the larger metamaterial area intersects with more electromagnetic waves even propagate out of the PAMS. Beside this, the results of each arrangement are better than that of two arrays of metamaterial with large distance. As the distance between the arrays decreases, the superstrate behaves as a homogeneous material at least for some particular frequency bands of the EM waves radiated from patch antenna.

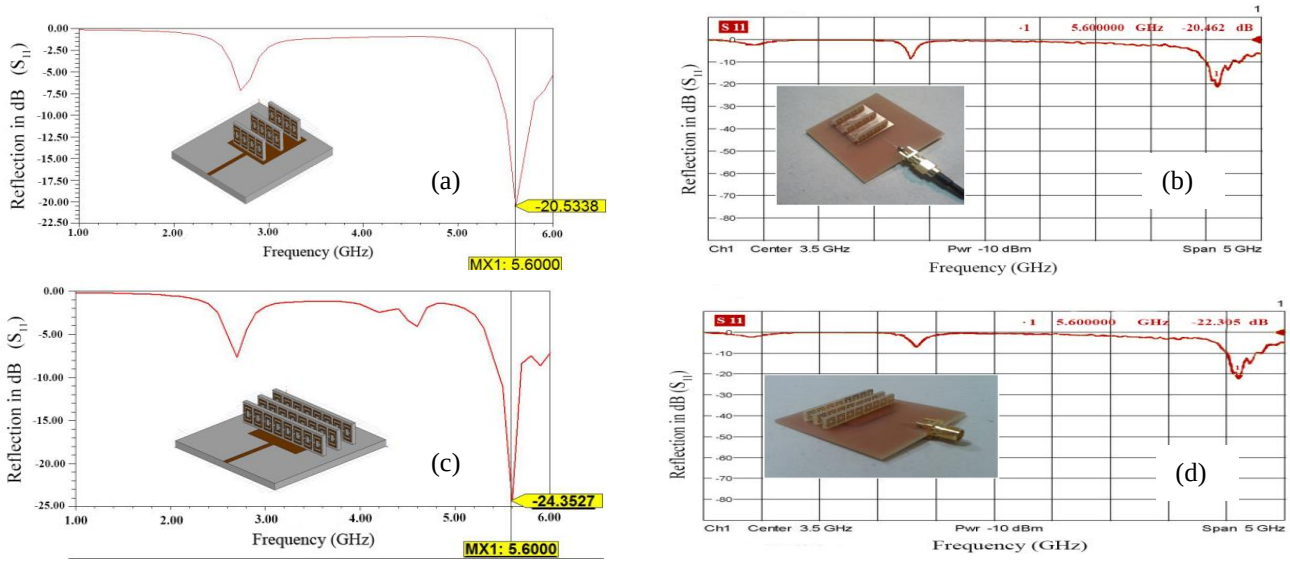

Fig. 9. Return loss of three arrays of metamaterials in the border in HFSS (a) and in measurement (b), return loss of three arrays of metamaterials exceed the border in HFSS (c) and in measurement (d).

5. Radiation properties of The PAMS

It is well known that the Voltage Standing Wave Ratio (VSWR) is an indication of the impedance matching between antenna and superstrate. A high VSWR is an indication that the signal is reflected prior to being radiated by the antenna. Both VSWR and return loss are different types of measuring and defining the antenna performance. The return losses of the PAMS and patch antenna are compared. On the other hand, VSWR result of the PAMS is also necessary to decide the antenna performance. The VSWR of metamaterial with seven array is calculated by Ansys HFSS and plotted as shown in Fig. 10. Although most of the commercial antennas are specified with 1.5:1 or less VSWR over some bandwidth, the VSWR of the PAMS is only 1.005 at 5.6GHz.

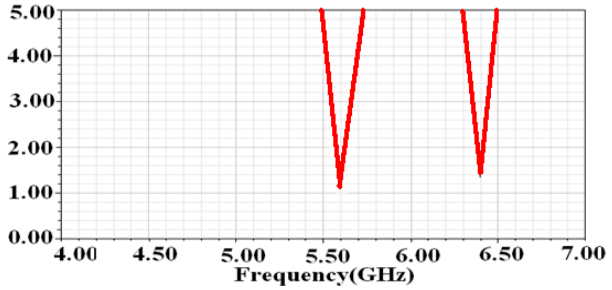

Fig. 10. VSWR of the PAMS with seven arrays of MTM.

The enhancement of return loss and VSWR is not exactly sufficient to decide the antenna performance. The radiation pattern of an antenna generally represents its most basic characteristics, since it determines the distribution of radiated energy into the space. Gain depends on directivity and directivity is totally depends on the shape of the radiation pattern of an antenna. Therefore the radiation patterns of the patch antenna and PAMS must also be compared at the same frequency to have exact decision on PAMS advantages. The airbox is assigned with a quarter-wavelength long of the frequency of interest in the direction of the radiated field in HFSS simulation. Since the gain of the radiation of the microstrip patch antenna is concentrated at broadsides, a rectangular box enclosing the patch antenna and PAMS is sufficient; the height of the airbox is 13.4 mm. Except for the bottom face, all of the faces are assigned as radiation boundary and bottom face is defined as finite conductivity copper.

The E and H plane radiation patterns of the patch antenna and PAMS are evaluated by HFSS at 5.6 GHz and plotted. E and H planes are obtained for different values of theta at fixed value of phi. H and E- plane simulated radiation patterns of microstrip patch antenna fed by a microstrip line are shown in Fig. 11. H-plane patterns (transmitted or received) are obtained by plotting the radiation pattern as a function of theta with respect to phi=90^o at 5.6 GHz. On the other hand, E-plane patterns are obtained by plotting the radiation pattern as a function of theta with respect to phi=0^o. The patch antenna behaves as omnidirectional with a gain of -4 dB for all theta values except for θ=90^o as shown in the H plane. The radiation pattern shape of the patch antenna at θ =90^o is similar to a dipole antenna with a maximum gain of -68 dB. The gain of the PAMS is much better than that of the patch antenna for H plane. The gain of the PAMS for θ=90^o is about 11.20 dB and have dipole type radiation pattern. The antenna radiation of PAMS is improved at all theta values with respect to patch antenna without metamaterial. The E plane radiation pattern of the patch antenna and the PAMS is also shown in Fig. 11. There is no significant change in the gain and radiation pattern of each antenna in the E plane.

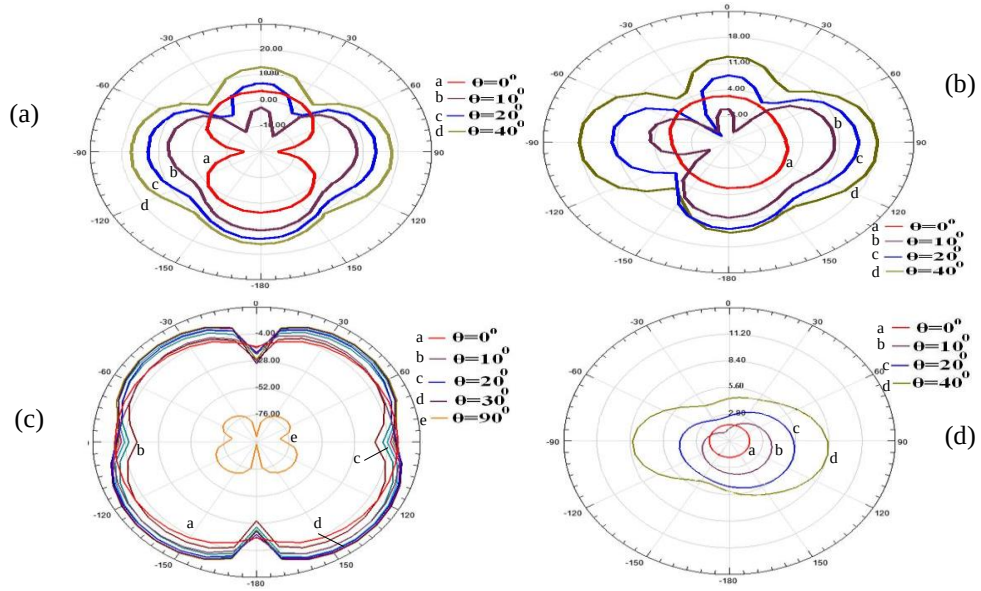

Fig. 11. Simulated H plane radiation pattern for patch antenna (a) and PAMS (b); E-plane radiation pattern for patch antenna (c) and PAMS (d) fed by a microstrip line.

The optimized PAMS operates at 5.6 GHz frequency has a simulated broadside gain of 9.44 dBi which is higher than that of patch antenna having 7.1 dBi. It should be pointed out that direct comparison between the gain of the PAMS and the patch antenna without metamaterial actually is not correct due to the presence of the metamaterial superstrate. Therefore, the operation of the PAMS is defined better by evaluating the maximum broadside gain with respect to the effective radiation aperture;

$$G_{max} = \left(\frac{4\pi}{\lambda_o}\right) A_{eff}\, e_{eff} = 9.44\text{dBi} \quad (4)$$

Where A_{eff} is the effective aperture size of the metamaterial superstrate (50mm×50mm) and e_{eff} is the radiation efficiency. Hence, the broadside gain of the PAMS operating at 5.6 GHz is 9.44 dBi. This means the most of the radiated wave is guided along the broadside direction.

6. Conclusion

We have proposed a double negative metamaterial inspired structure as a superstrate for antenna gain and radiation enhancement. Both simulations and measurements have demonstrated that the effective refractive index of the metamaterial composed of SRR-SW inclusions is negative at a frequency of 5.6 GHz. To validate the metamaterial effect, a patch antenna and different arrays of metamaterial superstrate working at this frequency have been simulated and fabricated. The simulation and measurement results have shown notable gain enhancement at the working frequency of the superstrate. Especially, the PAMS with 7 arrays of metamaterial working at 5.6 GHz has a 9.44 dBi gain enhancement at broadside direction with respect to the patch antenna without metamaterial, which is 72% of the radiation of a radiating surface with the same area. Owing to the PAMS, a second resonant frequency of the antenna is observed at 3 GHz with an effective size reduction of 53.571% compared to the original loop antenna.

It is possible to mention about two main advantages of PAMS. The first one is much better return loss at 5.6 GHz as shown in Table 2. While the measurement return loss of the patch antenna without metamaterial is -18.70 dB, that of the PAMS is -32.17 dB. This also proves efficiency of the PAMS. As a second advantage, the gain of the patch antenna with metamaterial is much better than that of the patch antenna without metamaterial for H plane as shown in Fig. 11. Radiation enhancement is observed for all values of theta. Hence the PAMS systems have possible potential usage areas such as airborne, spacecraft applications, GPS receivers and other mass produced wireless products.

References

[1] M. Karaaslan, E. Unal, E. Tetik, K. Delihacioglu, F. Karadag, F. Dincer, IET Microwaves Antennas and Prop., **7:3**, 215 (2013).
[2] A. Alu, F. Bilotti, N. Engheta, L. Vegni, IEEE Antennas and Wireless Propagation, **55**, 13 (2007).
[3] H. A. Majid, M. K. A. Rahim, Asia-Pacific Conference on Applied Electromagnetics Proceedings, 1-4 (2007).
[4] X. H. Song, W. Y. Wu, T.-G. Shen, Y. Q. Zhou, Optik, **122**, 1426 (2011).
[5] J. A. Fladie, J. T. Bernhard, IEEE Antennas and Wireless Propagation Letters, **5**, 563 (2006).
[6] H. A. Majid, M. K. Rahim, T. Masri, Progress In Electromagnetics Research M, **8**, 235 (2009).
[7] T. C. Han, M. K. A. Rahim, T. Masri, M. N. A. Karim, Proceedings of Asia-Pacific Microwave Conference, 1-4 (2007).
[8] A. M. Nicolson, G. F. Ross, IEEE Transactions on Instrumentation and Measurement, **19**, 377 (1970).
[9] W. B. Weir, Proceedings of the IEEE, **62**, 33 (1974).
[10] Microstrip Antennas: The Analysis and Design of Microstrip Antennas and Arrays, Edited by D. M. Pozar and D. H. Schaubert, NewJersey, United States (1995).

*Corresponding author: eunal@mku.edu.tr